Biological Trace Element Research (2024) 202:1084–1102
https://doi.org/10.1007/s12011-023-03745-6

RESEARCH

Testicular Toxicity in Rats Exposed to $AlCl_3$: a Proteomics Study

Huixin Peng[1,2] · Yanxin Huang[1,2] · Guangji Wei[1,2] · Yanfang Pang[1,2] · Huixiong Yuan[1,2] · Xiong Zou[3] · Yu'an Xie[3] · Wencheng Chen[1,2]

Received: 12 April 2023 / Accepted: 22 June 2023 / Published online: 29 June 2023

Abstract

Aluminum contamination is a growing environmental and public health concern, and aluminum testicular toxicity has been reported in male rats; however, the underlying mechanisms of this toxicity are unclear. The objective of this study was to investigate the effects of exposure to aluminum chloride ($AlCl_3$) on alterations in the levels of sex hormones (testosterone [T], luteinizing hormone [LH], and follicle-stimulating hormone [FSH]) and testicular damage. Additionally, the mechanisms of toxicity in the testes of $AlCl_3$-exposed rats were analyzed by proteomics. Three different concentrations of $AlCl_3$ were administered to rats. The results demonstrated a decrease in T, LH, and FSH levels with increasing concentrations of $AlCl_3$ exposure. HE staining results revealed that the spermatogenic cells in the $AlCl_3$-exposed rats were widened, disorganized, or absent, with increased severe tissue destruction at higher concentrations of $AlCl_3$ exposure. Kyoto Encyclopedia of Genes and Genomes (KEGG) and Gene Ontology (GO) enrichment analyses revealed that differentially expressed proteins (DEPs) after $AlCl_3$ exposure were primarily associated with various metabolic processes, sperm fibrous sheath, calcium-dependent protein binding, oxidative phosphorylation, and ribosomes. Subsequently, DEPs from each group were subjected to protein-protein interaction (PPI) analysis followed by the screening of interactional key DEPs. Western blot experiments validated the proteomics data, revealing the downregulation of sperm-related DEPs (AKAP4, ODF1, and OAZ3) and upregulation of regulatory ribosome-associated protein (UBA52) and mitochondrial ribosomal protein (MRPL32). These findings provide a basis for studying the mechanism of testicular toxicity due to $AlCl_3$ exposure.

Keywords $AlCl_3$ · Testis · Proteomics · TMT · Toxicity

Introduction

The total aluminum ore resource in the world amounts to 40−50 billion tons. Aluminum is used in various aspects of our daily life, including construction, household appliances, automobiles, and shop windows [1]. Moreover, the use of aluminum-containing AI products is on the rise. Furthermore, due to the low production cost, lightweight, and malleability of aluminum, the use of aluminum products in daily life is increasing. Due to the extensive use of aluminum products, these products are discarded into the environment, including the land, sea, and forest ecosystems [2, 3]. In addition, once aluminum enters the land ecosystem, it can cause acidification, yield reduction, and nutrient imbalance in the soil [4]. A study conducted on the rivers around Xi'an, China, reported a 2000-fold increase in aluminum concentration compared to the levels present six years ago. This undoubtedly jeopardizes the health of people who consume water from these rivers [5]. Biotoxicity due to aluminum exposure has raised global concern.

Numerous results have confirmed that aluminum exposure is toxic to the nervous, nephrology, myocardial toxicity, and reproductive systems [6–8]. However, the mechanisms of reproductive toxicity remain unclear. The toxicity mechanism of aluminum to humans is challenging to investigate directly.

Huixin Peng, Yanxin Huang and Guangji Wei contributed equally to this work.

✉ Yu'an Xie
215597239@qq.com

✉ Wencheng Chen
chwch3268@sina.com

1 The Affiliated Hospital of You jiang Medical University for Nationalities, Baise 533000, Guangxi, China

2 Graduate School of You jiang Medical University for Nationalities, Baise 533000, Guangxi, China

3 Guangxi Key Laboratory of reproductive health and birth defect prevention, Nanning 530000, Guangxi, China

However, since rats have biological characteristics similar to humans, we conducted an experiment exposing rats to $AlCl_3$ to explore its reproductive toxicity. We have previously reported that $AlCl_3$ exposure decreases sperm quality and viability in rats [9]. In another study of aluminum-exposed voles, sperm quality decreased significantly [10]. Some researchers have hypothesized that reproductive toxicity due to aluminum exposure may be related to oxidative stress and hormonal disorders [11, 12]. mRNA undergoes multiple regulatory processes during translation into protein; hence, mRNA levels alone do not accurately reflect body changes during a stress response. Proteomics is a research methodology based on high-throughput analytical and detection techniques. It is used to probe novel molecular markers and the effects of pollutants on organisms since it is the most widely used histological platform that allows in-depth studies on complex organisms and tissue proteins assessment qualitatively and quantitatively [13, 14]. Bioinformatics is a field that utilizes artificial intelligence to analyze and interpret biological data through computer technology. Therefore, as rats have biological characteristics similar to humans, this study exposed rats to $AlCl_3$ to explore its reproductive toxicity. Moreover, regarding $AlCl_3$ exposure to rat testicular tissue, proteomic sequencing and bioinformatics were employed to gain insights into the alterations in proteins. Studies have evaluated the toxic effects of pollutants on organisms by proteomics and bioinformatics, including the toxicity of nano plastics on algal proliferation, chromium-induced kidney toxicity, toxicity of fluoride to the mouse liver, and the biological toxicity of humic acid on fish [15–18]. Neurotoxicity due to aluminum exposure has been studied by incorporating proteomics aluminum-exposed rat models; however, to the best of our knowledge, no proteomic studies of testicular toxicity due to $AlCl_3$ exposure have been conducted. Therefore, evaluating testicular toxicity due to $AlCl_3$ exposure by proteomics is of great importance.

Aluminum chloride ($AlCl_3$), a widely used aluminum compound in daily human life, was used in this study to reveal the molecular mechanisms of testicular toxicity in $AlCl_3$-exposed rats. Proteomic analysis was performed for four groups with different exposures: control, low dose, medium dose, and high dose. Furthermore, bioinformatics analysis was performed to validate some DEPs that are closely related to reproduction using western blot. Our study of testicular toxicity due to $AlCl_3$ exposure contributes to a better understanding of the potential effects of $AlCl_3$ exposure on male reproduction and provides new molecular targets for $AlCl_3$ exposure reproductive toxicity.

Materials and Methods

Reagents and Materials

Aluminum trichloride hexahydrate ($AlCl_3$·6H2O) (Shanghai Aladdin Biochemical Technology Company (L1706080)); AKAP4 (PA5-109377) and ODF1 (PA5-69988) (Thermo Fisher); and NDUFAB1 (53896-1), MRPL32 (53101-1), LGALS4 (30034-1), and UBA52 (43827-1) were purchased from Signalway Antibody (SAB), and OAZ3 (orb215187) (Boster) was used in the study. FSH (MM-7086R2), LH (MM-0624R2), and T (MM-0577R2) were purchased from MEIMIAN.

Animal Experimental Design

Twenty-four 8-week-old male rats weighing 180–200 g that underwent five weeks of adaptive growth were randomly assigned to four groups, each group containing six rats. $AlCl_3$ was dissolved in distilled water. Based on the study by Xu et al. [19], the median lethal dose (LD_{50}) of $AlCl_3$ to rats, the daily body weight and water intake were considered to determine the amount of $AlCl_3$ that should be exposed to rats using the drinking water method. Four groups were formed based on these criteria: a high-dose group [1/5 LD_{50}, 256.72 mg/(kg·d)], a medium-dose group [1/10 LD_{50}, 128.36 mg/(kg·d)], a low-dose group [1/20 LD_{50}, 64.18 mg/(kg·d)], and control group [0 mg/(kg·d)]. The rats were kept under controlled environmental conditions with a temperature of 25±2 °C, relative humidity between 50% and 70%, and a 12 h light/dark cycle. The rats were fed standard rat feed (Table 1) and were provided with water containing $AlCl_3$ for a period of 16 weeks, which is equivalent to two rat spermatogenic cycles of rats. Subsequently, euthanasia with an injection of 200 mg/kg pentobarbital sodium was performed, following which intracardiac blood samples and bilateral testicular tissues were obtained and centrifuged to acquire the serum for sex hormone detection. Additionally, one part of the testicular tissue was fixed with 4% paraformaldehyde tissue fixative solution for histopathological evaluation, while the other part was stored in a −80 °C refrigerator for subsequent quantitative proteomic analysis and western blot detection. All animal procedures were approved by the Experimental Animal Use Ethics Committee of You jiang Medical College for Nationalities.

Quantitative Proteomics Analysis

The tissues were ground in liquid nitrogen to perform quantitative proteomics, and the supernatant was collected for protein extraction. The protein concentration was measured using the BCA protein kit. Subsequently, proteolytic digestion was performed. Impurities in the 200 μg protein were removed using an ultrafiltration tube, followed by the addition of iodoacetamide to block the reduction process. After washing, the trypsin digestion agent was added and centrifuged at 12,000 rpm for 20 min to collect the peptides. Each

Table 1 Product ingredient (content per kilogram of feed)

Moisture ≤100 g	Histidine ≥4.0 g	Iron ≥100 mg	Vitamin B1 ≥8 mg
Crude protein ≥180 g	Tryptophan ≥1.9 g	Manganese ≥75 g	Vitamin B2 ≥10 mg
Crude fat ≥40 g	Phenylpropyl + tyrosine ≥11.0 g	Copper ≥10 mg	Vitamin B6 ≥6 mg
Crude fiber ≤50 g	Threonine ≥6.5 g	Zinc ≥30 mg	Niacin ≥45 mg
Crude ash content ≤80 g	Leucine ≥14.4 g	iodine≥0.5 mg	Pantothenic acid ≥17 mg
Calcium 10–18 g	Isoleucine ≥7.0 g	Selenium ≥01–0.2 mg	Folic acid ≥4 mg
Total phosphorus 6–12 g	Valine ≥8.4 g	Vitamin A ≥7000IU	Biotin ≥0.10 mg
Lysine ≥8.2 g	Magnesium ≥2.0 g	Vitamin D ≥800 IU	Vitamin B12 ≥0.02 mg
Methionine + cystine ≥ 5.3 g	Potassium ≥5.0 g	Vitamin E≥60 IU	Choline ≥1250 mg

sample peptide was labeled using TMT, equilibrated using TMT reagent, and lysed using isopropanol. Furthermore, 100 μg of sample peptide was added to the solubilized TMT reagent, and the reaction was terminated by adding 100 μl of pure water after 2 h, followed by centrifugation of the sample to dry the bottom of the tube. The dried sample peptides were subjected to the AKTA Purifier100 system. The labeled peptides were separated using SCX chromatography, where peptide samples were subjected to acidification and loaded onto the sample column. After elution and desalting, samples were collected after centrifugation. Finally, LC-MS/MS analysis was performed. Sample peptides were redissolved in formic acid and attached to the analytical column for separation, followed by mass spectrometry analysis.

Bioinformatics Analysis

The identified proteins were classified using UniProt (https://www.uniprot.org/) database, and GO is an international set of classification systems for the functional description of genes. The different proteins coordinate with each other to perform their functions, and thus, classified DEPs were subjected to GO analysis. Subsequently, pathway enrichment analysis of differentially expressed genes was performed using the KEGG analysis (http://www.genome.jp/kegg/). Proteins consist of structural domains, and characterizing these domains is important to help understand their function. The structural domains of DEPs were annotated using Interproscan. Proteins are sorted into individual organelles after ribosome synthesis using protein sorting signals, and understanding the subcellular localization of proteins is crucial for the functional understanding of the organism. The subcellular localization of DEPs was obtained through the Cell-mPLOC 2.0 website. The PPI network was obtained by the STRING online analysis system (https://cn.string-db.org/cgi/input?sessionId). The PPI networks on the STRING system were analyzed using Cytoscape analysis software to obtain PPI network maps. Finally, the protein-protein interaction network (PPI) was used to analyze the interactions between DEPs.

Serum T, LH, and FSH Concentrations Were Measured Using ELISA

The rat serum was collected, and follicle-stimulating hormone (FSH), luteinizing hormone (LH), and testosterone (T) were determined using an ELISA reagent kit. Briefly, 10 μL of the sample was added to a 96-well plate along with 40 μL of sample diluent in each well. Additionally, 100 μL of HRP-labeled antibody was added to each well and incubated at 37 °C for 60 min. Following this, the liquid was discarded and the plate was washed five times using a wash solution. Subsequently, the substrate was added to each well, and the plate was incubated in the dark for 15 min at 37 °C. Finally, the stop solution was added, and a multifunctional microplate reader was used to detect the optical density (OD) value at 450 nm.

HE Staining

The fixed testicular tissue was dehydrated using a tissue dehydrator. Following dehydration, the tissue was embedded in a paraffin block and sectioned into 4–5-micron sections. Paraffin sections were dewaxed in xylene (I) and xylene (II) for 15 min, respectively. Subsequently, the sections were hydrated in 100%, 95%, 85%, and 75% ethanol solutions for 3 min each, followed by immersion in distilled water for 10 min. Finally, the sections were stained with hematoxylin for 5 min to visualize the nuclei. The excess staining solution was removed by gentle rinsing with tap water. The sections were then subjected to 1% hydrochloric acid alcohol fractionation for 5 s, followed by ammonia-alcohol bluing for about 10 s. After wiping the excess water off the slides, the samples were stained in eosin stain for 5 min. The slides were again rinsed with tap water, and the excess water was wiped off. The samples were observed under a microscope, adjusting the staining as required. Finally, the stained tissue sections were placed in an oven at 37 °C for 30 min to ensure evaporation of the water. The sections were then successively incubated with xylene (I) and xylene (II) for 3 min each and then sealed with neutral resin. Micrographs were

captured using an optical microscope to assess pathological features. The evaluation process involved randomly selecting 10 fields at 20× magnification to assess four pathological criteria, namely basement membrane separation, immature cell presence in the spermatogenic tubule lumen, spermatogenic tubule degeneration, and atrophy. The severity of each criterion was scored from 0 to 3, with 0 indicating the absence of the phenomenon, 1 indicating a mild occurrence, 2 indicating a more pronounced occurrence, and 3 indicating an obvious phenomenon. To evaluate the results, Johnsen scoring (JS) was performed on 40 randomly selected seminiferous tubules in each group using an optical microscope, following the criteria outlined in Table 2 [20].

Determination of Testis Morphology

Germinal epithelial thickness (GET) was determined by measuring the longest and shortest distances of epithelial thickness in cross-sections of the spermatogenic tubule, which was followed by mean value calculation. The mean distance of the length and width of the spermatogenic tubule was measured to determine the diameter of the tubule (STD). Germinal cell degeneration was evaluated based on the statistical values of GET and STD [21].

Western Blot

Protein lysate (containing PMSF) was added according to the weight of the rat testis tissue. Then, the protein was extracted, and its concentration was detected according to the BCA Protein Quantitation Kit. Next, appropriate gels matched to the different molecular weight sizes were selected. The sample was then added, which was followed by electrophoresis, transmembrane, and blocking. Finally, the first antibody was added and incubated overnight before adding the second antibody. The bands were developed on a chemiluminescent developer and analyzed for grayscale values using ImageJ v 1.8.0.

Table 2 Johnsen's score used to evaluate testicular biopsies (JS)

	Score description
1	No cells
2	Sertoli cells without germ cells
3	Only spermatogonia
4	Only a few spermatocytes
5	Many spermatocytes
6	Only a few early spermatids
7	Many early spermatids without differentiation
8	Few late spermatids
9	Many late spermatids
10	Full spermatogenesis

Statistical Analysis

SPSS 25 was utilized to analyze the collected data, which was observed to follow a normal distribution and exhibit homogeneity of variance. One-way analysis of variance and post hoc Tukey's tests were employed to assess the data. The results are presented as mean ± standard deviation. For data that did not follow a normal distribution or exhibited uneven variance, Kruskal–Wallis and Mann–Whitney U tests were used, and the results were reported as median (min-max). GraphPad Prism (version 9.0) was used for data visualization. Furthermore, a P value of <0.05 was considered statistically significant.

Results

Data Quality Control of Proteins

Based on the proteomic analysis, 7860 proteins were detected in rat testicular tissues. Three biological replicates were detected, and further quantitative analysis was performed. A total of 7859 proteins were detected in the control group, and 7859, 7852, and 7852 proteins were detected in the low-, medium-, and high-dose groups, respectively. As seen in Fig. 1A,B, 90.59% of proteins weighed more than 10 kDa, and more than 91.64 of the proteins had at least two peptides. This indicated that the quality of our data set was excellent. Additionally, the results of the PCA (Fig. 1C) show that the difference between the control and low-dose groups was not significant; however, a significant difference was present between the control and medium-dose group.

Identification of Deferentially Expressed Proteins after $AlCl_3$ Exposure to Testicular Tissue

Using volcano plots, we expressed the DEPs that were at the intersection of the control group versus the low-mid-high, the control group versus the mid-high, and the control group versus the low-mid-high group, respectively, after $AlCl_3$ exposure. There were 59 DEPs in the control group compared with the low-dose group, 31 of which were upregulated and 28 were downregulated (Fig. 2A). There were 121 DEPs in the control group compared with the medium-dose group; 39 were upregulated, and 82 were downregulated (Fig. 2B). Sixty-nine DEPs were present in the control group compared with the high-dose group; 26 were upregulated, and 43 were downregulated (Fig. 2C). Sixty-six DEPs were present in the conjoint analysis between the control group and low- and medium-dose

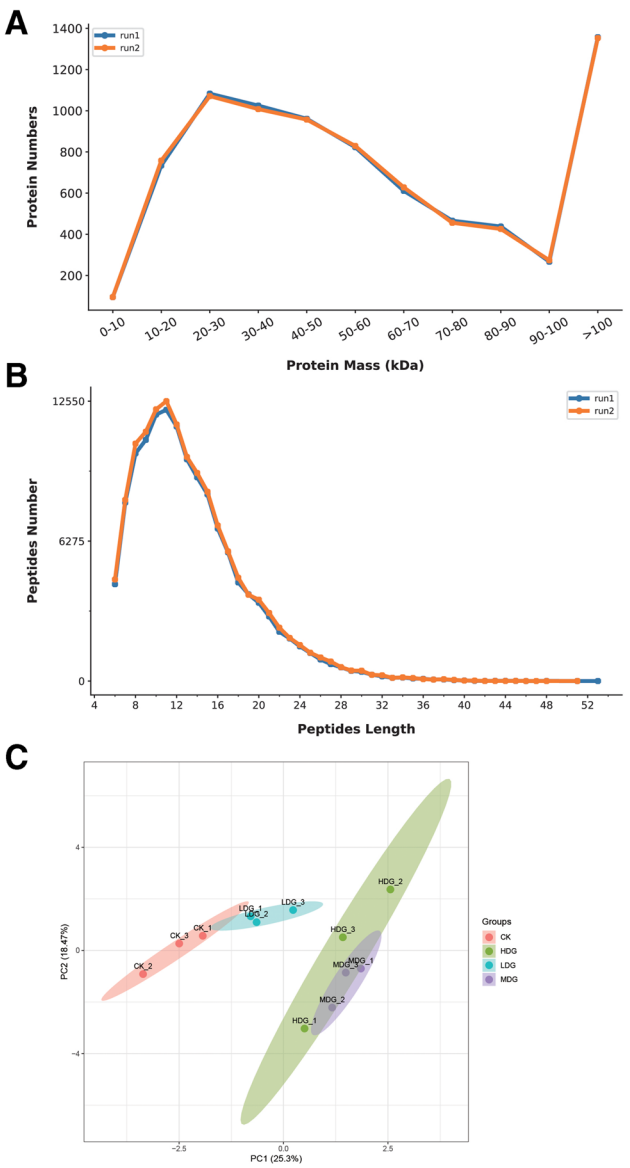

Fig. 1 (**A**) Protein molecular weight statistics. (**B**) Number of peptides contained in the identified protein. (**C**) Protein PCA graph

groups; 31 of them were upregulated, and 35 were downregulated (Fig. 2D). Ninety-six DEPs were present in the conjoint analysis between the control group and medium- and high-dose groups; 40 were upregulated, and 56 were downregulated (Fig. 2E). Sixty-eight DEPs were in the conjoint analysis between control and low-mid-high-dose groups; 34 were upregulated, and 34 were downregulated (Fig. 2F; Fig. 3).

Gene Ontology (GO) Functional Annotation of DEP

DEPs were subjected to GO functional annotation (Fig. 4). The biological processes most enriched by DEPs included a variety of metabolic processes such as aspartate family amino acid catabolic process (GO:0009068), retinol metabolic process (GO:0042572), nucleotide-sugar metabolic process (GO:0009225), and melanin metabolic process (GO:0006582), as well as regulation of cytoplasmic translation (GO:2000765) and protein hexamerization (GO:0034214). The affected cellular components included ribosome (GO:0005840), rough endoplasmic reticulum (GO:0005791), sperm fibrous sheath (GO:0035686), sperm connecting piece (GO:0097224), and sperm flagellum (GO:0036126). Additionally, the molecular functions of intramolecular oxidoreductase activity, transposing C=C bonds (GO:0016863), calcium-dependent protein binding (GO:0048306), structural constituent of ribosome (GO:0003735), and nucleoside triphosphate diphosphatase activity (GO:0047429) were affected.

KEGG Pathway Enrichment Results of DEPs

The KEGG (Fig. 5A–F) pathway enrichment analysis was performed for these DEPs. The results showed that the most enriched pathways were glycine, serine, and threonine metabolism, oxidative phosphorylation, ribosome signaling pathway, etc.

Structural Domain Enrichment of DEPs

Structural domain enrichment analysis enables an understanding of proteins functions and identification of proteins associated with $AlCl_3$ exposure leading to testicular toxicity. Through (Fig. 6A–F) structural domain enrichment, we found that the most affected proteins were acyl carrier protein (ACP), ribosomal protein L27e, ribosomal protein L31e, ribosomal protein L32p, and ribosomal protein L40e. These may be some of the key targets of testicular toxicity due to $AlCl_3$ exposure.

Subcellular Localization Analysis of the DEPs

Subcellular localization analysis was also performed for each group of differential proteins (Fig. 5A–F), and we found that the top-ranked proteins affected after $AlCl_3$ exposure were cytosolic, cytoplasmic, and mitochondrial proteins.

PPI Analysis of DEPs

To investigate the relationship between DEP interactions obtained from the four groups, PPI networks of DEPs were established by combining each concentration group with the control group, as well as by combining multiple groups with the control group. Spermatogenesis-related proteins (Oaz3, ODF1, and AKAP4) were found to be tightly linked, and their expression was downregulated. Furthermore, molecules related to oxidative phosphorylation (NDUFAB1) regulated

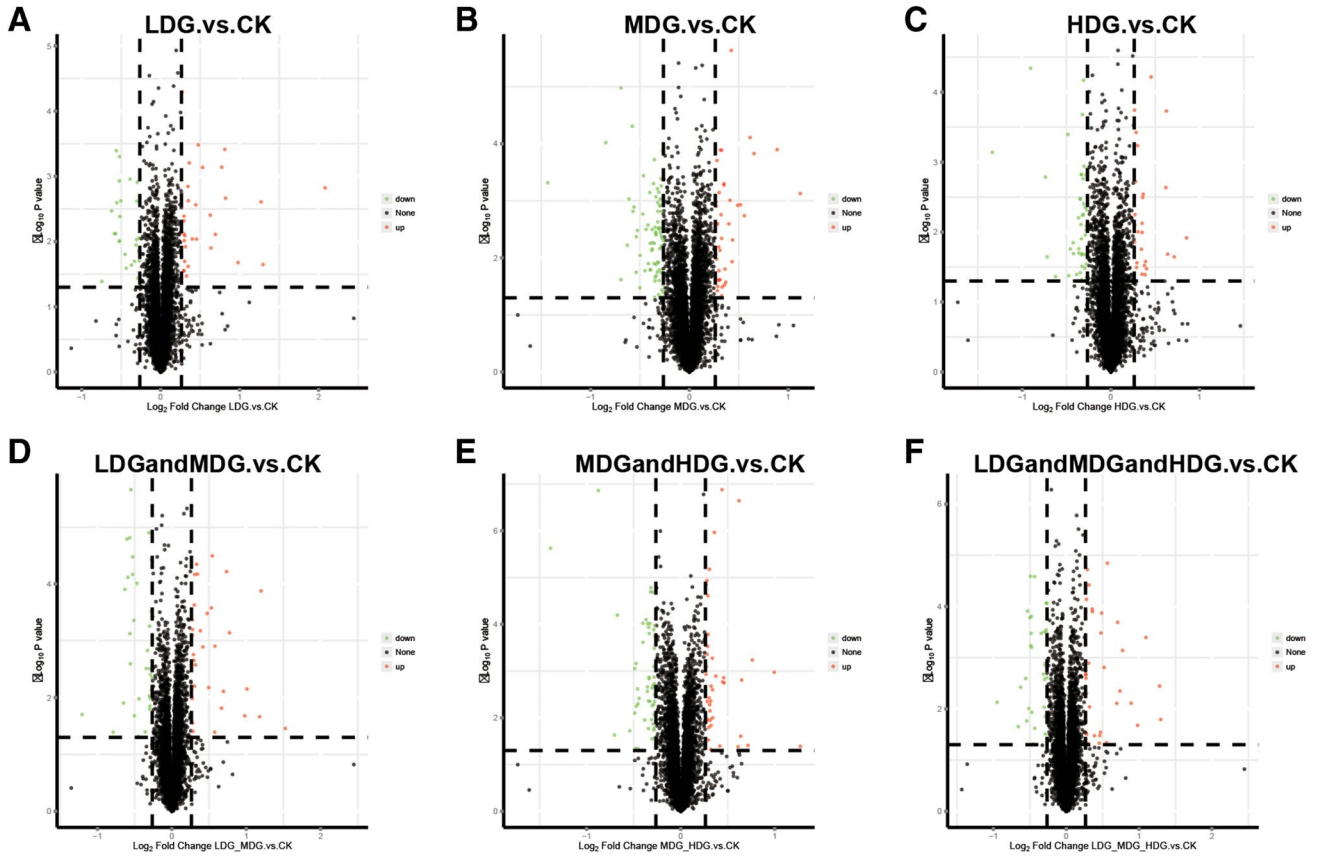

Fig. 2 Volcano plots according to the deferentially expressed proteins (DEPs): (**A**) control vs. low-dose group; (**B**) control vs. medium-dose group; (**C**) control vs. high-dose group; (**D**) control vs. low- and medium-dose group; (**E**) control vs. medium- and high-dose group; (**F**) control vs. low-, medium-, and high-dose group

the ribosome-associated protein UBA52 and the mitochondrial ribosomal protein MRPL32, which interacted directly or indirectly in the PPI network of each group. NDUFAB1 protein expression was downregulated, while the expression of UBA52 and MRPL32 was upregulated.

Serum T, LH, and FSH

Exposure to $AlCl_3$ resulted in a decrease in reproductive hormones, which was dependent on increasing concentrations of $AlCl_3$ exposure. Statistically significant differences were observed in LH and FSH levels between the high-dose group exposure and the control group. However, there were no significant differences between the low- and medium-dose groups and the control group in terms of LH and FSH levels. Compared with the low-dose group, the high-dose group displayed a significant decrease in LH and FSH ($P < 0.05$). Additionally, T levels between the low-dose group and the control group did not differ significantly. However, significant differences were observed between the medium- and high-dose groups and the control group ($P < 0.05$). Notably, the high-dose group exhibited a more significant decrease than the low-dose and medium-dose groups.

HE Histopathological and Morphological Evaluation Results

HE staining revealed (Fig. 9D; Table 3) that the seminiferous tubules in the control group were regularly arranged with a normal basement membrane and a large number of spermatogenic cells. However, in the $AlCl_3$ exposure groups, the seminiferous tubules were irregularly arranged, with a reduced number of spermatogenic cells, and were degenerated and atrophic. Additionally, tissue destruction was more severe in the high-dose group compared to the low- and medium-dose groups. Furthermore, the levels of STD, GET, and JS in the testicular tissue of the $AlCl_3$ exposure groups were significantly lower compared to the control group ($P < 0.05$) (Table 4). Notably, the high-dose group exhibited a more significant decrease than the low-dose group ($P < 0.05$).

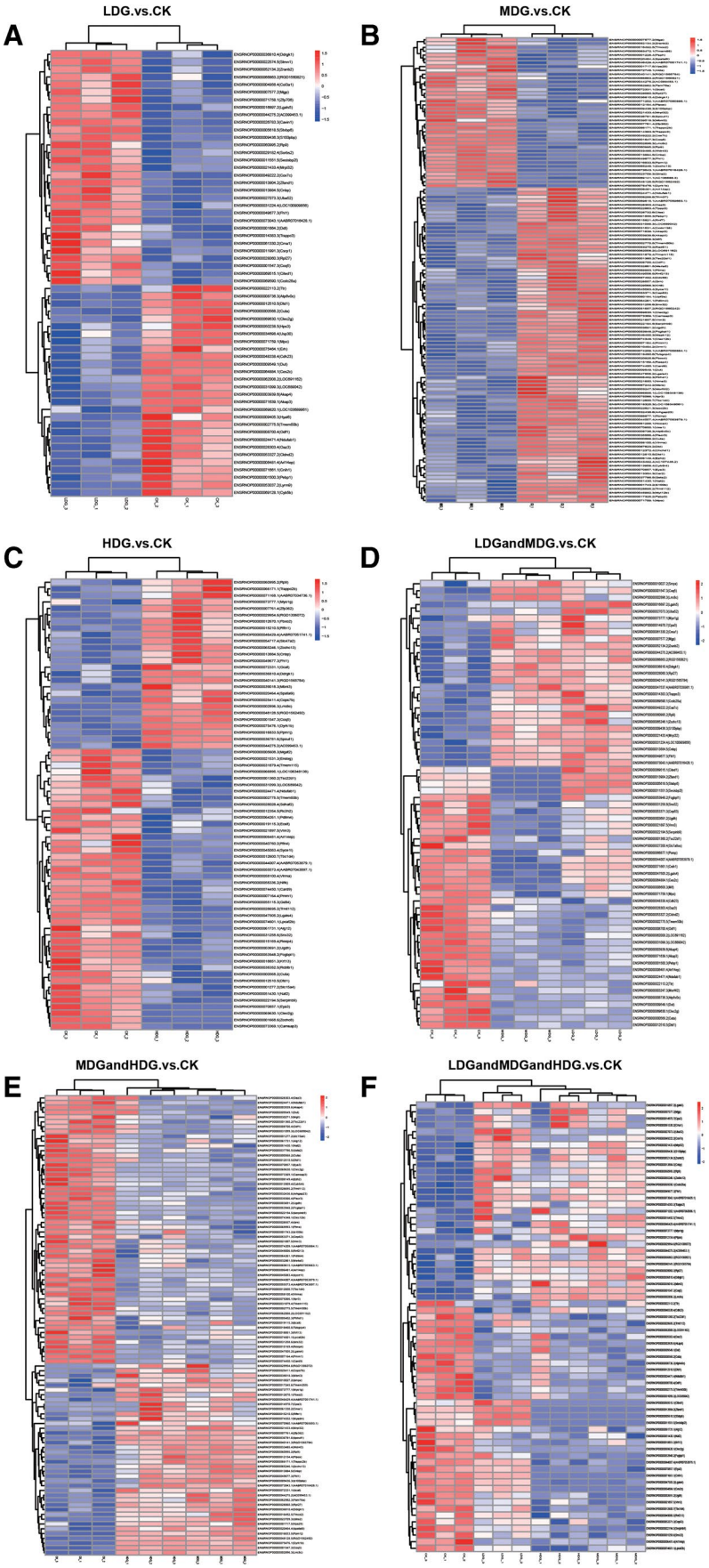

Fig. 3 Heat map of the DEPs: (**A**) control vs. low-dose group; (**B**) control vs. medium-dose group; (**C**) control vs. high-dose group; (**D**) control vs. low- and medium-dose group; (**E**) control vs. medium- and high-dose group; (**F**) control vs. low-, medium-, and high-dose group

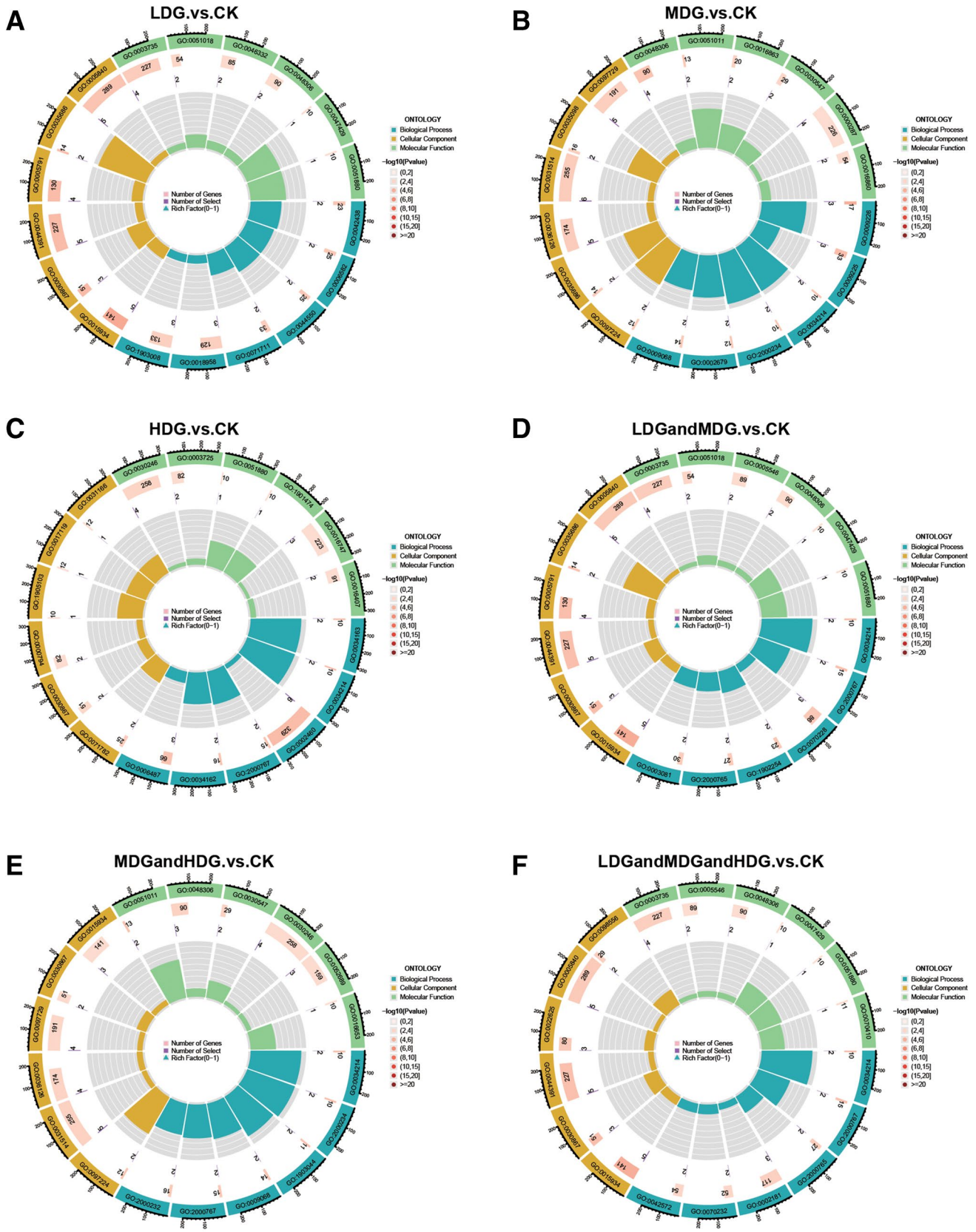

Fig. 4 Histogram of the GO enrichment analysis: (**A**) the control group with the low-dose group; (**B**) the control group with the medium-dose group; (**C**) the control group with the high-dose group; (**D**) the control group with the low- and medium-dose groups; (**E**) the control group with the medium- and high-dose groups; (**F**) the control group with the low-, medium-, and high-dose groups

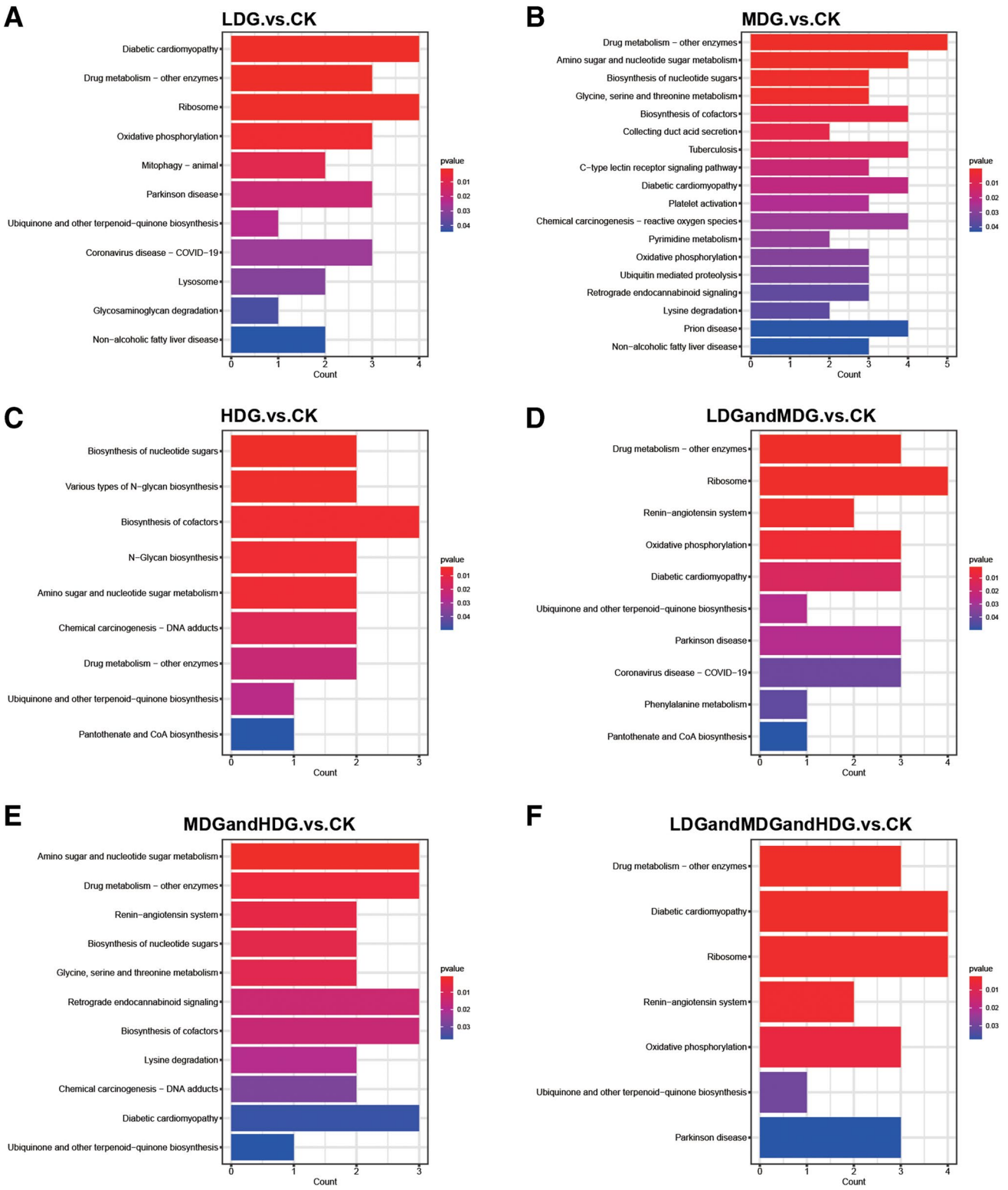

Fig. 5 The KEGG enrichment results: (**A**) the control group with the low-dose group; (**B**) the control group with the medium-dose group; (**C**) the control group with the high-dose group; (**D**) the control group with the low- and medium-dose groups; (**E**) the control group with the medium- and high-dose groups; (**F**) the control group with the low-, medium-, and high-dose groups

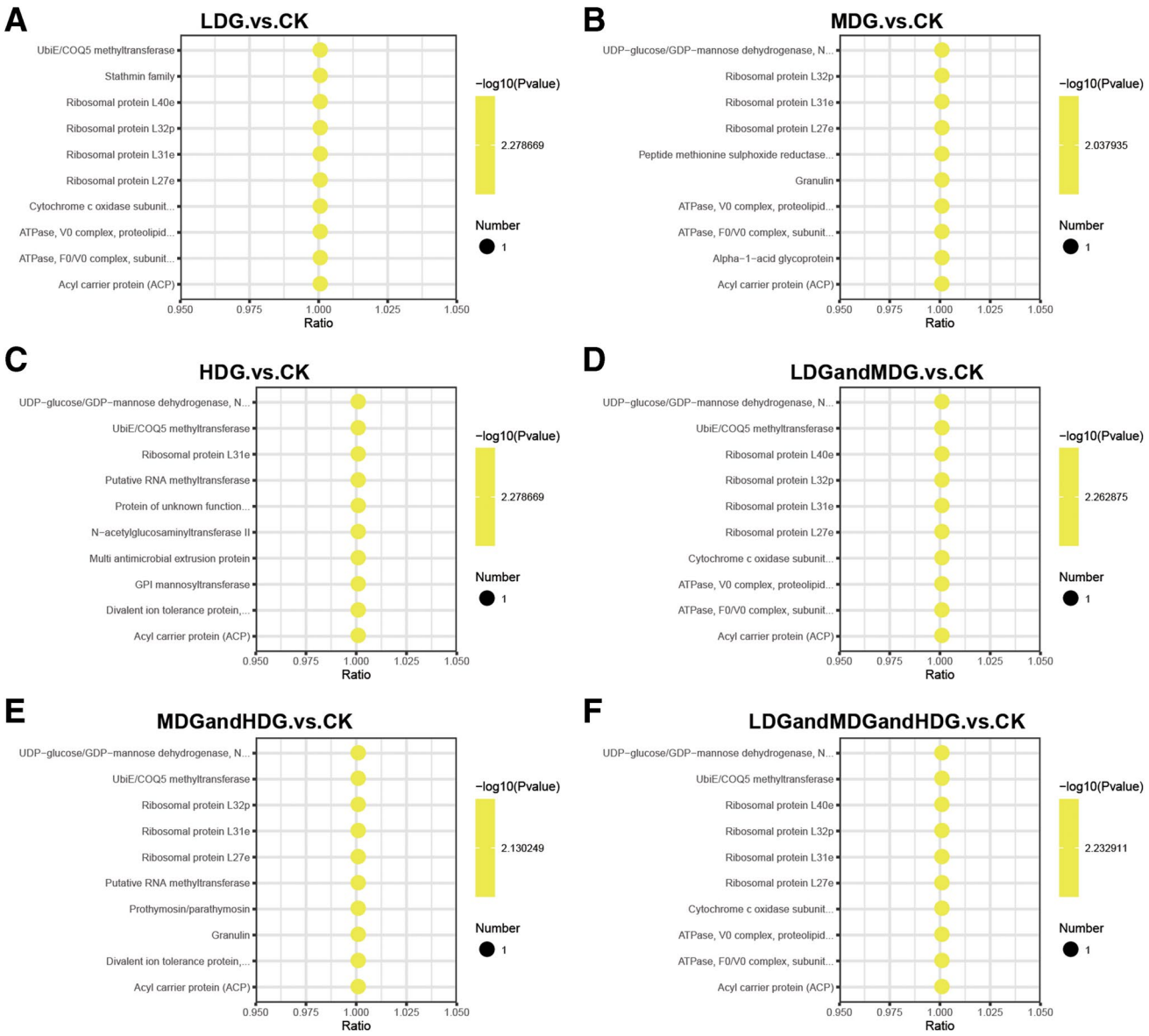

Fig. 6 Differential protein structural domain enrichment analysis: (**A**) control vs. low-dose group; (**B**) control vs. medium-dose group; (**C**) control vs. high-dose group; (**d**) control vs. low- and medium-dose groups; (**E**) control vs. medium- and high-dose groups; (**F**) control vs. low-, medium-, and high-dose groups

Western Blot

To validate the accuracy of the proteomic data, western blot experiments were performed for AKAP4, ODF1, OAZ3, NDUFAB1, Mrpl32, Lgals4, and UBA52. The proteomic data analysis was consistent with the western blot results. After $AlCl_3$ exposure, the expression levels of five proteins, including AKAP4, ODF1, OAZ3, NDUFAB, and Lgals4, were downregulated with increasing concentrations of $AlCl_3$ exposure compared to the control group. The genes AKAP4, ODF1, and OAZ3 were downregulated in the low-, medium- and high-dose groups. Additionally, the low-dose group exhibited downregulation of these genes compared to the medium- and high-dose groups ($P < 0.05$). NDUFAB1 and Lgals4 were downregulated in the control group compared to the low-, middle- and high-dose groups ($P < 0.05$). Compared to the high-dose group, they were downregulated in the low-dose group ($P < 0.05$) but showed no significant difference between the low- and middle-dose group. Moreover, exposure to increasing concentrations of $AlCl_3$ resulted in an upregulation of UBA52 protein expression. The control group exhibited significantly higher levels of UBA52 expression compared to the middle- and high-dose groups, whereas the low-dose group showed significantly higher

Table 3 Histopathological evaluation results of testicular tissue after exposure to different $AlCl_3$ (ten fields were randomly selected at 20× magnification)

	Control ($n = 6$)	Low-dose group ($n = 6$)	Medium-dose group ($n = 6$)	High-dose group ($n = 6$)	P*
Basement membrane separations	0.00 (0.00–1.00)	2.00 (1.00–3.00) [a]	2.00 (1.00–3.00) [a]	2.00 (1.00–3.00)[a]	<0.05
Presence of immature cells in the lumen	1.00 (0.00–1.00)	1.00 (1.00–3.00)	2.00 (1.00–3.00)[a]	2.00 (2.00–3.00)[a]	<0.05
Degeneration of seminiferous tubules	0.00 (0.00–2.00)	1.00 (1.00–3.00)	2.00 (1.00–3.00)[a]	2.50 (2.00–3.00)[a]	<0.05
Atrophy of seminiferous tubules	1.00 (0.00–1.00)	1.00 (0.00–3.00)	2.00 (1.00–3.00)[a]	3.00 (2.00–3.00)[a,b]	<0.05

Data are presented as median (min–max)

[a]Compared with the control group ($p < 0.05$)

[b]Compared with the low-dose group ($p < 0.05$)

P* Kruskal–Wallis

Table 4 Histomorphometric evaluation of testicular tissue after exposure to different concentrations of $AlCl_3$

	Control	Low-dose group	Medium-dose group	High-dose group	P*
STD	316.05 ± 30.09	302.43 ± 25.30	234.91 ± 17.48[a,b]	219.85 ± 17.48[a,b]	<0.05
GET	117.68 ± 9.20	111.93 ± 7.14	79.88 ± 8.92[a,b]	73.41 ± 6.35[a,b]	<0.05
JS	9.68 ± 0.26	9.39 ± 0.35	6.77 ± 0.48[a,b]	6.46 ± 0.37[a,b]	<0.05

Data are presented as mean ± standard deviation

[a]Compared with the control group ($P < 0.05$)

[b]Compared with the low-dose group ($P < 0.05$)

STD seminiferous tubule diameter, *GET* germinal epithelial thickness, *JS* Johnsen's score

expression levels compared to the high-dose group. Additionally, the medium-dose group demonstrated significantly higher expression of Mrpl32 compared to both the control and low-dose groups ($P < 0.05$). These findings validate the accuracy of our proteomic data. Furthermore, $AlCl_3$ exposure resulted in the upregulation or downregulation of these proteins, thereby inducing testicular damage and sperm quality decline and ultimately leading to reproductive damage in rats.

Discussion

The reproductive toxicity induced by aluminum in humans has garnered significant attention. Our findings indicate that exposure to $AlCl_3$ resulted in irregularly arranged seminiferous tubules and a decrease in the number of spermatogenic cells compared to the control group. Additionally, immature cells were observed in the lumen, the seminiferous tubules showed signs of degeneration and atrophy, and the basement membrane was shed, ultimately leading to a reduction in sperm count. Notably, increasing $AlCl_3$ concentration was observed to worsen these features. Furthermore, hormones related to male reproduction were also downregulated in the rat models. To explore the mechanism of testicular toxicity caused by $AlCl_3$, we used proteomic tools. Proteomics is a powerful tool to assess $AlCl_3$ exposure-related toxicity in rat testes and is widely used in toxicological studies. In this study, a gradient of toxicity exposure was set up, wherein three doses (low, medium, and high) were compared with the control. Additionally, a joint comparison was performed between multiple groups to obtain credible and accurate results. A low-dose exposure was associated with mild damage and a small number of DEPs; therefore, this data was not considered when a combined analysis of the medium- and high-dose groups was performed. However, comprehensive analysis can reveal the mechanism of the joint effect of $AlCl_3$ exposure from low to high doses. The reliability of our protein sequencing is validated by the fact that more than 91.64 proteins had shown at least two peptides (Fig. 1A–C). Additionally, PCA indicated differences between the groups after $AlCl_3$ exposure, further confirming the reliability of our sequencing results. The DEPs detected were expressed in the form of a volcano diagram (Fig. 2), which presents the up and downregulated proteins. The top-ranked genes were displayed in the form of a heat map (Fig. 3). Through a comprehensive analysis of our proteomic results data, we suggest that further research on $AlCl_3$-induced testicular toxicity should focus on the metabolic processes of amino acids, oxidative phosphorylation, ribosome signaling pathways, and organelle damages, such as mitochondrial and ribosomal damages. Furthermore, with an increase in $AlCl_3$

exposure, the hormone related to male reproduction was also downregulated. We will combine the above points to discuss.

Metabolic Processes

After exposure to $AlCl_3$, GO enrichment analysis (Fig. 4A–F) revealed that the DEPs were related to the catabolic processes of the aspartate family amino acids (GO:0009068) and the metabolic processes of retinol (GO:0042572) and melanin (GO:0006582). Previous studies report that retinol is a crucial element in regulating testicular function and sperm production. It is particularly important for the development of germ cells from mitosis to meiosis and the regulation of testicular function. Moreover, the absence of retinol can result in Leydig cell differentiation impairment, leading to reproductive function damage [20, 21]. Another study revealed a correlation between the metabolism of melanin and T [22]. Moreover, recent studies indicate that D-aspartate, a physiological amino acid found mainly in the pituitary gland and testis, can stimulate the release of LH and T when it is administered as sodium D-aspartate. Endogenous D-aspartate was reported to be present in the advanced stages of spermatogenesis, including spermatocytes and spermatozoa. It stimulated spermatogenesis indirectly through the hypothalamic-pituitary-gonadal axis [23, 24]. Notably, $AlCl_3$ exposure induces testicular toxicity and significantly affects the metabolic processes. Amino acid transport and metabolism play a crucial role in the normal functioning of the organism, and amino acids are similar to other important molecules, such as hormones and growth factors, that are involved in the regulation of the organism through specific pathways [25]. Adequate amino acids are required for proper growth, development, and reproduction. Additionally, the quality of amino acids has also been reported to affect reproduction in Drosophila [26]. The study found that exposure to $AlCl_3$ resulted in a decrease in reproductive-related hormones, with the most significant decrease observed at the highest exposure concentration. This was accompanied by histological damage to the testis (Fig. 9A–D). Similar results were observed in mice exposed to arsenic trioxide, where a decrease in testosterone was noted [27]. Additionally, a decrease in FSH has been linked to a decline in sperm count [28]. Recent studies have suggested that L-arginine supplementation may reverse reproductive toxicity caused by aluminum exposure. This supplementation can restore sex hormone levels to normal, improve sperm motility to some extent, and reduce testicular tissue edema and interstitial tissue congestion caused by aluminum exposure. Thus, normal metabolism of amino acids is important for male reproductive function [29]. KEGG analysis revealed that DEPs were enriched in glycine, serine, and threonine metabolic pathways (Fig. 5A–F). Our findings suggest that aluminum exposure may negatively affect amino acid metabolism, which could lead to impaired metabolic pathways that affect sex hormone levels and testicular function in rats. These results are consistent with our previous study, which showed a decrease in semen quality in rats [9].

Signaling Pathways

The calcium signaling pathway has been demonstrated to regulate spermatogenesis and sperm maturation in mammals, amphibians, and other animals [30, 31]. GO enrichment of the DEPs revealed enrichment in calcium-dependent protein binding (GO:0048306) (Fig. 4). Additionally, the KEGG pathway enrichment of DEPs revealed the presence of the calcium signaling pathway (Fig. 5). These findings suggest that changes in calcium-dependent protein binding can induce cytotoxicity [32, 33]. In the calcium signaling pathway, the entry of calcium ions entry into the cell causes a sudden increase in intracellular calcium ion concentration and activation of downstream response mechanisms (e.g., CaMKII, nitric oxide synthase, and calcium-regulated neuronal phosphatase). Butylated hydroxyanisol is capable of disrupting calcium homeostasis to induce testicular toxicity [34]. Moreover, lysophosphatidic acid can improve sperm viability by activating L-type calcium channels [35]. Furthermore, sperm viability levels directly affect fertility [36]. These findings show that calcium signaling pathways have an important role in testicular toxicity and spermatogenesis, wherein calcium signaling pathways modulation can potentially improve testicular toxicity due to $A1C1_3$-induced testicular toxicity.

Oxidative Phosphorylation

Mitochondria have a bilayer membrane structure and carry out oxidative phosphorylation in their inner membrane. Oxidative phosphorylation is composed of five complexes, each working in concert to produce ATP [37]. Sodium fluoride and cadmium cause oxidative damage to the testes of silkworms and mice by affecting mitochondrial oxidative phosphorylation [38, 39]. When testicle torsion occurs, it interferes with oxidative phosphorylation and affects the mitochondria's energy supply [40]. Therefore, we can speculate that oxidative phosphorylation could be involved in $AlCl_3$-induced testicular toxicity. Our study revealed that after $AlCl_3$ exposure, a large proportion of DEPs were enriched in oxidative phosphorylation and affected mitochondrial proteins (Fig. 5). Additionally, the subcellular localization of DEPs was identified (Fig. 7). Further analysis of the protein-protein interaction (PPI) PPI of DEPs revealed that NDUFAB1, a molecule related to the oxidative phosphorylation pathway, was involved in the regulation of the PPI interaction network (Fig. 8). NDUFAB1 is a mitochondrial ACP essential for maintaining cell viability.

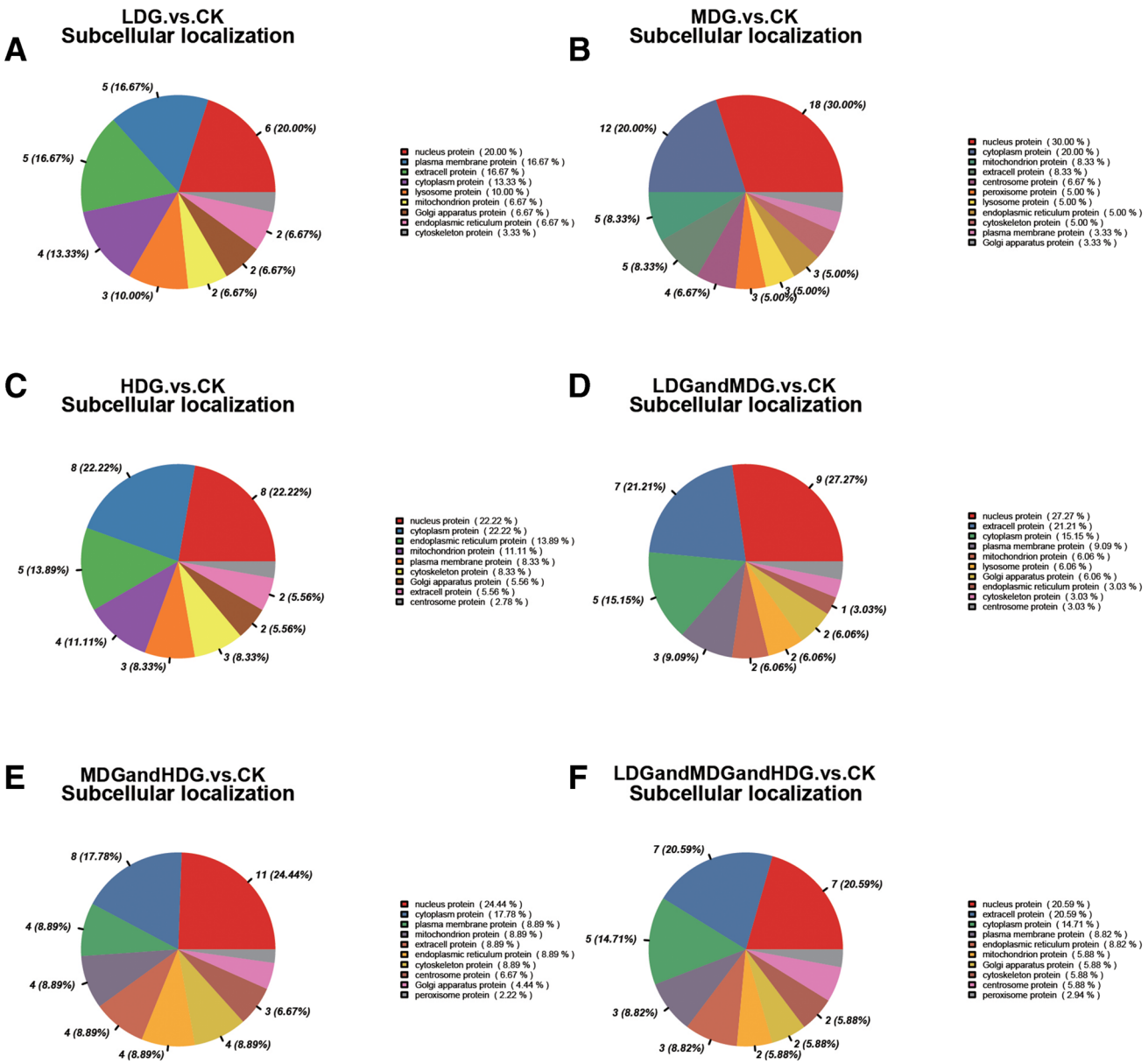

Fig. 7 Pie charts of the DEPs' subcellular localization: (**A**) control vs. low-dose group; (**B**) control vs. medium-dose group; (**C**) control vs. high-dose group; (**D**) control vs. low- and medium-dose groups; (**E**) control vs. medium- and high-dose groups; (**F**) control vs. low-, medium-, and high-dose groups

Interestingly, the ACP that appears in the structural domain enrichment results corresponds to NDUFAB1 (Fig. 6), whose functions are primarily involved in assembling mitochondrial respiratory chain complexes and mitochondrial ribosomes [41]. Moreover, NDUFAB1 can prevent obesity and insulin resistance by enhancing mitochondrial metabolism [42]. The overexpression of NDUFAB1 effectively enhances mitochondrial bioenergy and exerts a cardioprotective effect in the heart subjected to ischemic perfusion injury. Therefore, NDUFAB1 is a central target in reproductive toxicity due to $AlCl_3$ exposure [43]. However, the specific regulatory mechanism of NDUFAB1 in testicular toxicity due to $AlCl_3$ exposure is unclear.

Ribosomes

Ribosomes, composed of RNA and proteins, translate messenger RNA into encoded proteins in all living systems. Ribosomes are present in almost all cells and are considered the "molecular machinery" of the cell. The stability of ribosomal machinery is essential for cell proliferation [44]. This current study observed that exposure to $AlCl_3$ resulted

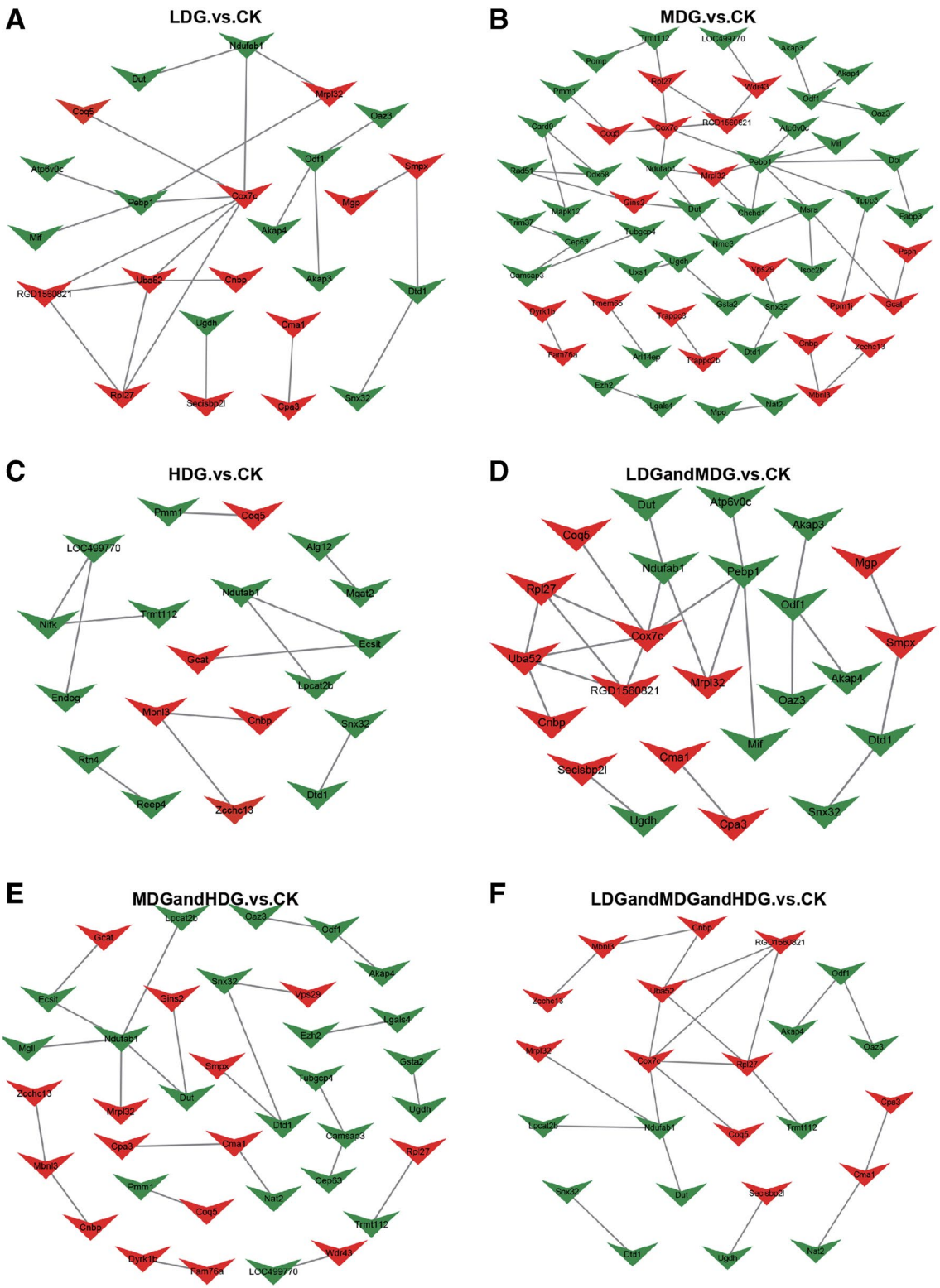

Fig. 8 Protein interaction network plots made by six sets of common DEPs in control, low-, medium-, and high-dose groups. Red is upregulated, and green is downregulated

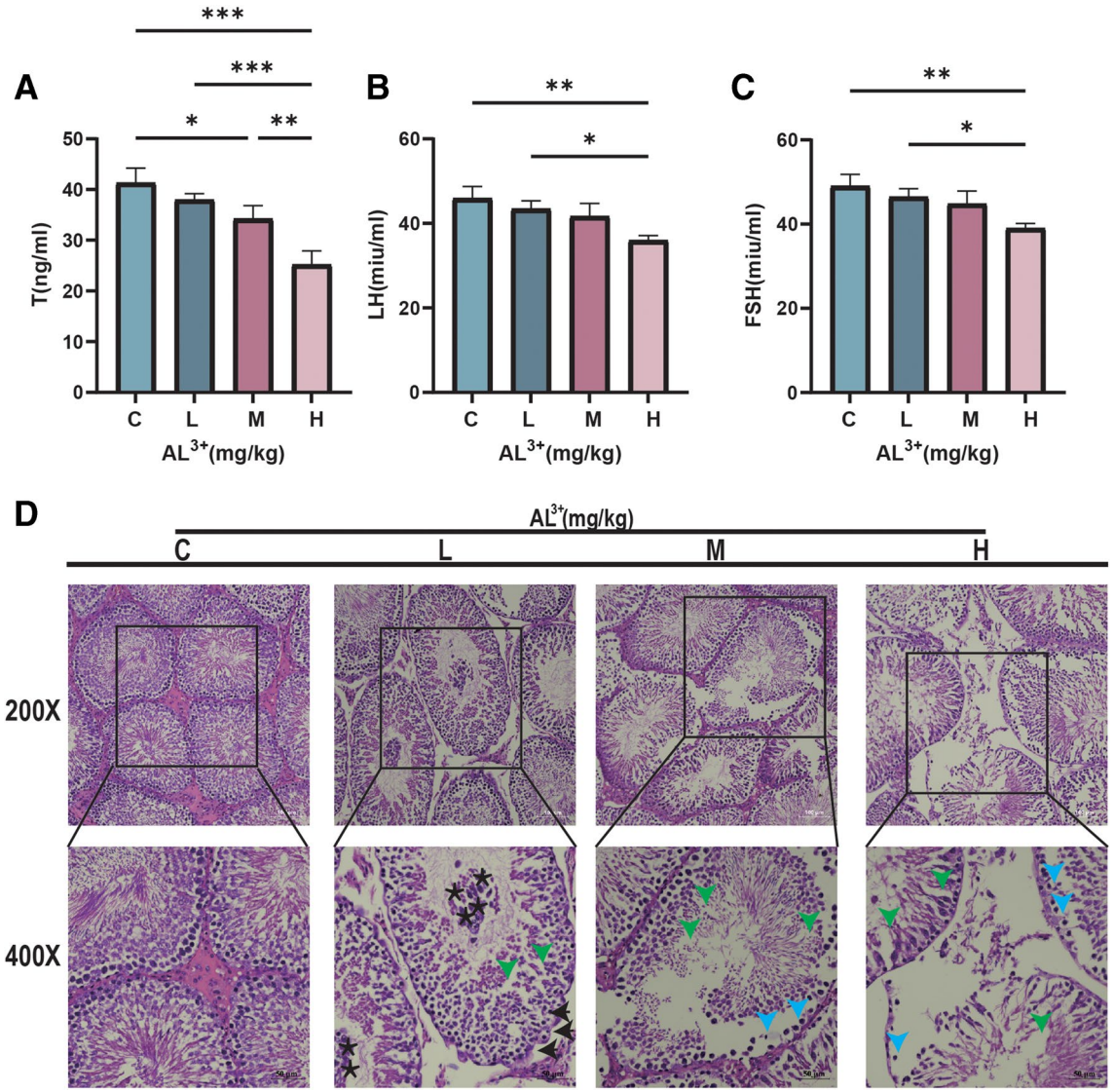

Fig. 9 FSH, LH, and T concentrations and testicular tissue damage in rats exposed to low, medium, and high concentrations of $AlCl_3$. **A**, **B**, and **C** denote T, LH, and FSH levels, respectively, and **D** represents HE staining observations. C: control group; L: low-concentration $AlCl_3$ exposure group; M: medium-concentration $AlCl_3$ exposure group; H: high-concentration $AlCl_3$ exposure group. ★: presence of immature cells in the lumen; black arrow: atrophy of seminiferous tubules; green arrow: degeneration of seminiferous tubules; blue arrow: basement membrane separations

in enriched DEPs that were specifically related to the ribosome (GO:0005840) and ribosome structural composition (GO:0003735) among others (Fig. 4). Additionally, KEGG enrichment analysis revealed the significant enrichment of DEPs in the ribosomal pathway (Fig. 5). The domain enrichment analysis further supported these findings, indicating that the most affected proteins were ribosomal proteins. High sugar intake has been reported to enhance the destruction of bisphenol A, leading to reproductive toxicity through the upregulation of ribosome-related genes [45]. Recent studies have highlighted the involvement of ribosome-related proteins, such as RPL23, RPS27A, and RPS27L, in regulating the cell cycle and apoptotic processes and inducing apoptosis [46]. Abnormal expression of mitochondrial ribosomal proteins (MRPs) can lead to mitochondrial metabolic disorders and cellular dysfunction. Moreover, MRPs can play an essential role in the regulation of cell death [47]. Recent studies have demonstrated that inhibition of MRPs, such as MRPL19 and MRPL32, increased cell viability and attenuated OGGR-induced apoptosis [48]. The ubiquitin A-52 residue ribosomal protein fusion product 1 (UBA52) is a ubiquitin-ribosome fusion gene. Its N-terminus contains ubiquitin, and the C-terminus contains 60S and RPL40. UBA52 has been shown to activate the RPL40-MDM2-p53

pathway, leading to cell cycle arrest and apoptosis [49]. These findings are consistent with our results. In the current analysis of DEPs using PPI networks, we observed that the ribosome-associated protein UBA52 and the mitochondrial ribosomal protein MRPL32 were upregulated and directly or indirectly interacted with other proteins in each group (Fig. 8). Western blot detection also revealed that the expression of UBA52 increased in correlation with $AlCl_3$ exposure concentration (Fig. 10G). The expression of UBA52 in the low-, middle- and high-dose groups showed a significant increase compared with the control group. Notably, the middle- and high-dose groups exhibited more significant changes in UBA52 expression compared to the low-dose group. The expression of MRPL32 was also observed to be significantly increased in the medium-dose group compared to the control group and low-dose group (Fig. 10C). This suggests that UBA52 and MRPL32 may cause testicular toxicity by affecting the stability of the ribosomal pathway. However, further experiments are required to fully understand the specific mechanism involved (Fig. 9).

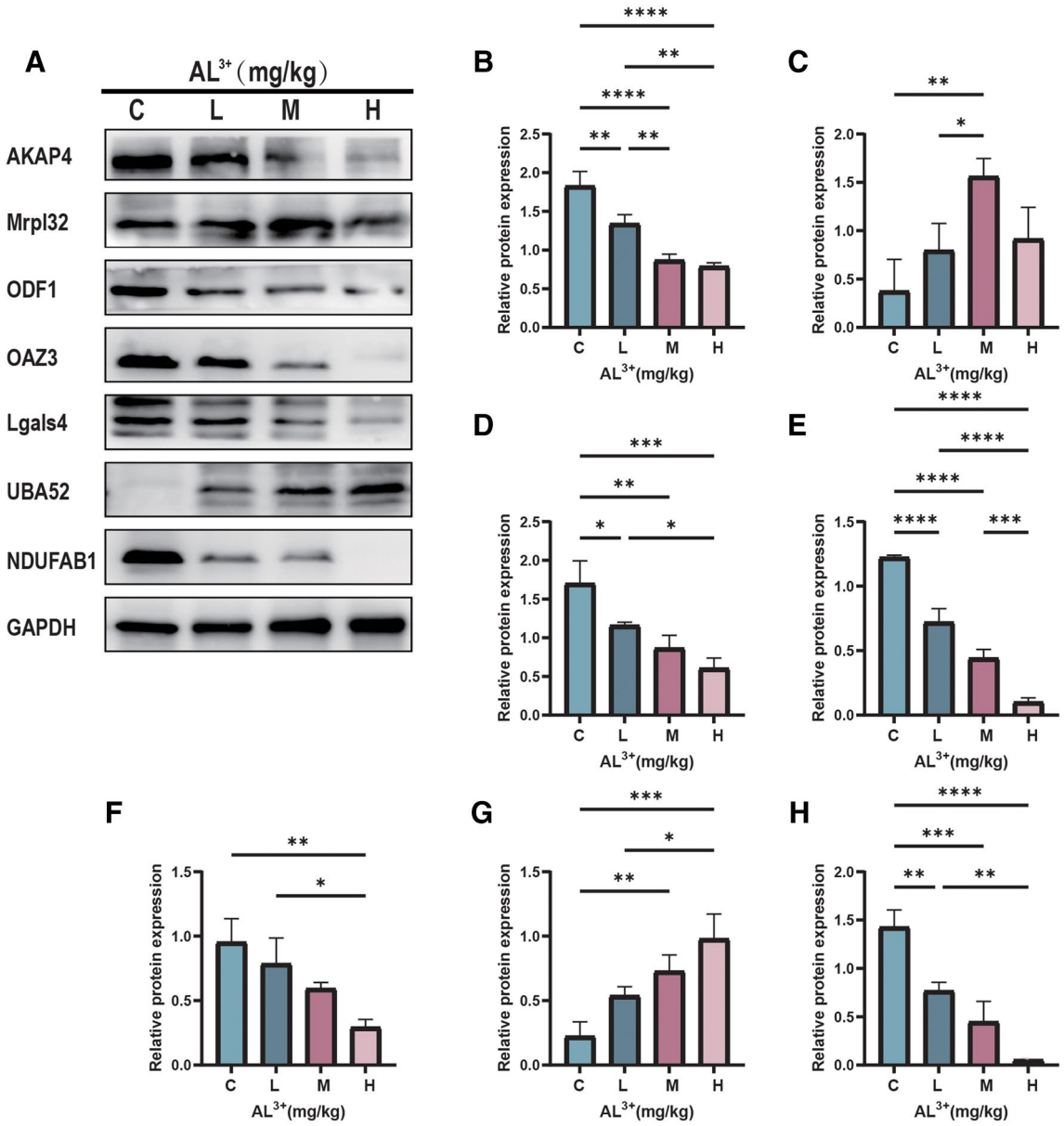

Fig. 10 (**A**) Plots of changes in AKAP4, Mrpl32, ODF1, OAZ3, Lgals4, UBA52, and NDUFAB1 protein expression after different concentrations of $AlCl_3$ exposure. (**B**–**H**) Quantification of protein expression for AKAP4, Mrpl32, ODF1, OAZ3, Lgals4, UBA52, and NDUFAB, respectively. All data are expressed as mean ± standard deviation. The asterisk (*) sign indicates statistical difference from control (*$P < 0.05$, **$P < 0.01$, ***$P < 0.001$, ****$P < 0.0001$)

Key Proteins

In our study, we conducted a multi-group DEPs GO enrichment analysis and discovered that the DEPs were linked to cellular components such as sperm fibrous sheath (GO:0035686), sperm linker (GO:0097224), and sperm flagella (GO:0036126) (Fig. 4). Additionally, we observed a strong correlation between the DEPs AKAP4, ODF1, and OAZ3, which are known to play a crucial role in male reproduction; hence, we focused on these proteins. A-kinase anchoring protein 4 (AKAP4) is the main component of the sperm's fibrous sheath and is related to sperm viability [50]. Knockdown of the AKAP4 gene in mice using CRISPR-Cas4 caused abnormal sperm morphology and poor viability [51]. The western blot analysis showed a decrease in AKAP4 expression in the $AlCl_3$ exposed groups compared to the control group (Fig. 10B). The decrease was most significant at the highest concentration of $AlCl_3$, and the downregulation was more prominent in the middle- and high-dose groups compared to the low-dose group. Thus, the expression of AKAP4 is dose-dependent in response to $AlCl_3$ exposure. These findings suggest that AKAP4 could potentially be a target for testicular toxicity induced by $AlCl_3$ exposure. The outer dense fibers 1 (ODF1) of the sperm tail, a filamentous structure located in the middle part of the mammalian sperm tail and the outer part of the main part of the axoneme, acts as a linker; in some males with infertility, abnormal sperm morphology occurs due to reduced ODF1 [52, 53]. Our study utilized proteomic data and western blot to confirm that exposure to $AlCl_3$ resulted in the downregulated expression of ODF1 in testis tissue (Fig. 10D). Specifically, the expression of ODF1 was decreased in the $AlCl_3$ exposure group compared to the control group, with the medium- and high-dose groups showing a more significant decrease than the low-dose group. However, further investigation is necessary to determine whether ODF1 is regulated by upstream genes. Ornithine decarboxylase antizyme 3 (OAZ3) is crucial in regulating cell growth and reproduction. OAZ3 is testis-specific, and its expression is restricted to haploid germ cells in the testis. As presented in Fig. 10E, the expression of OAZ3 decreased following $AlCl_3$ exposure. Notably, this decrease was more pronounced in the middle- and high-dose groups compared to the low-dose group. Additionally, there was a clear correlation between the decrease in OAZ3 expression and $AlCl_3$ exposure concentration. The knockdown of OAZ3 leads to sterility in male mice. Interestingly, a recent study demonstrated that OAZ3 is also involved in the formation of the sperm tail [54, 55]. Hence, it can be speculated that the target of reproductive toxicity induced by $AlCl_3$ exposure could be the sperm tail. Lipid rafts are highly dynamic and structurally heterogeneous regions in the cell membrane that facilitate molecular interactions and signal transduction between cells. Galectin-4 (Lgals4) has been reported to enhance the stability of lipid rafts. Research indicates that Lgals4 can also increase the expression of cyclin B1, thereby improving cell cycle progression [55, 56]. Our proteomics results indicate a significant downregulation of Lgals4, which was further validated using a western blot (Fig. 10F). The expression of Lgals4 was found to be inhibited upon exposure to $AlCl_3$, with a more significant reduction observed in the high-dose group compared to the low-dose group. However, further investigation is required to determine whether the downregulation of Lgals4 protein expression caused by $AlCl_3$ exposure leads to testicular injury. In summary, the mechanism of testicular toxicity induced by exposure to $AlCl_3$ is highly complex. Our study has only provided a preliminary exploration of the changes in protein molecules following exposure, and we intend to continue researching the regulatory mechanisms involved.

Conclusion

In summary, $AlCl_3$ exposure significantly disrupted the morphology of rat testicular tissue and affected the balance of blood hormones in rats, resulting in decreased blood levels of reproduction-related sex hormones, attenuated sperm viability in rats, and testicular damage. These effects may be related to sperm fibrous sheaths, sperm connection straps, spermatic flagella, calcium-dependent protein binding, amino acid metabolic pathways, calcium signaling pathways, oxidative phosphorylation, and ribosomal pathways. Structural domain enrichment and cellular sub-localization analyses of DEPs revealed that the targeted organelles of $AlCl_3$ exposure are mitochondria and ribosomes. Moreover, our western blot experiments validated the results. These results were consistent with the proteomic data. Our proteomic data and western blot experiments demonstrated the downregulation of sperm-related DEPs (AKAP4, ODF1, and OAZ3) and the upregulation of regulatory ribosome-associated protein (UBA52) and MPR (MRPL32). These findings suggest that these proteins may be molecular targets of $AlCl_3$ exposure leading to testicular toxicity.

Author Contributions Huixin Peng, Yanxin Huang, and Guangji Wei were responsible for experiment operation and paper writing; Yanfang Pang and Huixiong Yuan were responsible for animal feeding and modeling; Xiong Zou was responsible for partial data analysis; Wencheng Chen and Yu'an Xie were responsible for experiment design, paper writing guidance, overall framework construction, and project fund preparation.

Funding We thank the Guangxi Natural Science Foundation Project (2020GXNSFAA297257), Guangxi Science and Technology Program Project (21-220-22), Guangxi University Young and Middle-aged Teachers' Basic Ability Improvement Project (2020KY13017),

Guangxi Zhuang Autonomous Region Administration of Traditional Chinese Medicine Self-financing Scientific Research Project (GZZC2020248), and Guangxi Zhuang Autonomous Region Health and Health Commission Self-financing Scientific Research Course (Z20201416).

Data Availability All data will be provided upon request.

Declarations

Competing Interests The authors declare no competing interests.

References

1. Chen H, Chow CL, Lau D (2022) Deterioration mechanisms and advanced inspection technologies of aluminum windows. Materials 15:354. https://doi.org/10.3390/ma15010354
2. Chauhan DK, Yadav V, Vaculík M et al (2021) Aluminum toxicity and aluminum stress-induced physiological tolerance responses in higher plants. Crit Rev Biotechnol 41:715–730. https://doi.org/10.1080/07388551.2021.1874282
3. Liu Q, Zhou L, Liu F et al (2019) Uptake and subcellular distribution of aluminum in a marine diatom. Ecotoxicol Environ Saf 169:85–92. https://doi.org/10.1016/j.ecoenv.2018.10.095
4. Shetty R, Vidya CS-N, Prakash NB et al (2021) Aluminum toxicity in plants and its possible mitigation in acid soils by biochar: a review. Sci Total Environ 765:142744. https://doi.org/10.1016/j.scitotenv.2020.142744
5. Wang D, He Y, Liang J et al (2013) Distribution and source analysis of aluminum in rivers near Xi'an City, China. Environ Monit Assess 185:1041–1053. https://doi.org/10.1007/s10661-012-2612-2
6. Makhdoomi S, Ariafar S, Mirzaei F, Mohammadi M (2023) Aluminum neurotoxicity and autophagy: a mechanistic view. Neurol Res 45:216–225. https://doi.org/10.1080/01616412.2022.2132727
7. Ahmed WMS, Ibrahim MA, Helmy NA et al (2022) Amelioration of aluminum-induced hepatic and nephrotoxicity by Premna odorata extract is mediated by lowering MMP9 and TGF-β gene alterations in Wistar rat. Environ Sci Pollut Res 29:72827–72838. https://doi.org/10.1007/s11356-022-20735-8
8. Zhou L, He M, Li X et al (2022) Molecular mechanism of aluminum-induced oxidative damage and apoptosis in rat cardiomyocytes. Biol Trace Elem Res 200:308–317. https://doi.org/10.1007/s12011-021-02646-w
9. Yuan H-X, Pang Y-F, Wang J-L, Chen W-C (2019) Impacts of aluminum on sperm quality and sperm mitochondria in male rats. Zhonghua Nan Ke Xue 25:579–585
10. Miska-Schramm A, Kapusta J, Kruczek M (2017) The effect of aluminum exposure on reproductive ability in the bank vole (Myodes glareolus). Biol Trace Elem Res 177:97–106. https://doi.org/10.1007/s12011-016-0848-3
11. Cheraghi E, Golkar A, Roshanaei K, Alani B (2017) Aluminium-induced oxidative stress, apoptosis and alterations in testicular tissue and sperm quality in Wistar rats: ameliorative effects of curcumin. Int J fertil Steril 11. https://doi.org/10.22074/ijfs.2017.4859
12. da Silva LD, da Silva GL, de Sousa FE et al (2020) Aluminum exposure promotes histopathological and pro-oxidant damage to the prostate and gonads of male and female adult gerbils. Exp Mol Pathol 116:104486. https://doi.org/10.1016/j.yexmp.2020.104486
13. Rozanova S, Barkovits K, Nikolov M et al (2021) Quantitative mass spectrometry-based proteomics: an overview. Methods Mol Biol 2228:85–116. https://doi.org/10.1007/978-1-0716-1024-4_8
14. McArdle AJ, Menikou S (2021) What is proteomics? Arch Dis Child Educ Pract Ed 106:178–181. https://doi.org/10.1136/archdischild-2019-317434
15. Liu Z, Li Y, Sepúlveda MS et al (2021) Development of an adverse outcome pathway for nanoplastic toxicity in Daphnia pulex using proteomics. Sci Total Environ 766:144249. https://doi.org/10.1016/j.scitotenv.2020.144249
16. Sun X, Wang Y, Jiang T et al (2021) Nephrotoxicity profile of cadmium revealed by proteomics in mouse kidney. Biol Trace Elem Res 199:1929–1940. https://doi.org/10.1007/s12011-020-02312-7
17. Yurchenko VV, Morozov AA, Kiriukhin BA (2022) Proteomics analysis in Japanese Medaka Oryzias latipes exposed to humic acid revealed suppression of innate immunity and coagulation proteins. Biology (Basel) 11:683. https://doi.org/10.3390/biology11050683
18. Khan ZN, Sabino IT, de Souza Melo CG et al (2019) Liver proteome of mice with distinct genetic susceptibilities to fluorosis treated with different concentrations of F in the drinking water. Biol Trace Elem Res 187:107–119. https://doi.org/10.1007/s12011-018-1344-8
19. Xu F, Liu Y, Zhao H et al (2017) Aluminum chloride caused liver dysfunction and mitochondrial energy metabolism disorder in rat. J Inorg Biochem 174:55–62. https://doi.org/10.1016/j.jinorgbio.2017.04.016
20. Doyle TJ, Oudes AJ, Kim KH (2009) Temporal profiling of rat transcriptomes in retinol-replenished vitamin A-deficient testis. Syst Biol Reprod Med 55:145–163. https://doi.org/10.3109/19396360902896844
21. Yang Y, Luo J, Yu D et al (2018) Vitamin A promotes Leydig cell differentiation via alcohol dehydrogenase 1. Front Endocrinol 9:644. https://doi.org/10.3389/fendo.2018.00644
22. Béziers P, Ducrest A-L, Simon C, Roulin A (2017) Circulating testosterone and feather-gene expression of receptors and metabolic enzymes in relation to melanin-based colouration in the barn owl. Gen Comp Endocrinol 250:36–45. https://doi.org/10.1016/j.ygcen.2017.04.015
23. Topo E, Soricelli A, D'Aniello A et al (2009) The role and molecular mechanism of D-aspartic acid in the release and synthesis of LH and testosterone in humans and rats. Reprod Biol Endocrinol 7:120. https://doi.org/10.1186/1477-7827-7-120
24. Santillo A, Falvo S, Chieffi P et al (2016) D-aspartate induces proliferative pathways in spermatogonial GC-1 cells: GC-1 CELL PROLIFERATION INDUCED BY D-Asp. J Cell Physiol 231:490–495. https://doi.org/10.1002/jcp.25095
25. Morris MB, Ozsoy S, Zada M et al (2020) Selected amino acids promote mouse pre-implantation embryo development in a growth factor-like manner. Front Physiol 11:140. https://doi.org/10.3389/fphys.2020.00140
26. Ma C, Mirth CK, Hall MD, Piper MDW (2022) Amino acid quality modifies the quantitative availability of protein for reproduction in Drosophila melanogaster. J Insect Physiol 139:104050. https://doi.org/10.1016/j.jinsphys.2020.104050
27. Ommati MM, Heidari R, Zamiri MJ et al (2020) The footprints of oxidative stress and mitochondrial impairment in arsenic trioxide-induced testosterone release suppression in pubertal and mature F1-male Balb/c mice via the downregulation of 3β-HSD, 17β-HSD, and CYP11a expression. Biol Trace Elem Res 195:125–134. https://doi.org/10.1007/s12011-019-01815-2
28. Oduwole OO, Peltoketo H, Huhtaniemi IT (2018) Role of follicle-stimulating hormone in spermatogenesis. Front Endocrinol (Lausanne) 9:763. https://doi.org/10.3389/fendo.2018.00763
29. Ozcan Yildirim S, Colakoglu N, Ozer Kaya S (2022) Protective effects of L -arginine against aluminium chloride-induced

testicular damage in rats. Andrologia 54. https://doi.org/10.1111/and.14569
30. Gao D-D, Lan C-F, Cao X-N et al (2022) G protein-coupled estrogen receptor promotes acrosome reaction via regulation of Ca2+ signaling in mouse sperm†. Biol Reprod 107:1026–1034. https://doi.org/10.1093/biolre/ioac136
31. Sato T, Arimura T, Murata K et al (2021) Differences of extracellular cues and Ca2+ permeable channels in the signaling path differences ways for inducing amphibian sperm motility. Zoolog Sci 38:343–351. https://doi.org/10.2108/zs200159
32. Zhou F, Du G, Xie J et al (2020) RyRs mediate lead-induced neurodegenerative disorders through calcium signaling pathways. Sci Total Environ 701:134901. https://doi.org/10.1016/j.scitotenv.2019.134901
33. Ren T, Tang Y, Wang M et al (2020) Triptolide induces apoptosis through the calcium/calmodulin-dependent protein kinase kinaseβ/AMP-activated protein kinase signaling pathway in non-small cell lung cancer cells. Oncol Rep. https://doi.org/10.3892/or.2020.7763
34. Ham J, Lim W, You S, Song G (2020) Butylated hydroxyanisole induces testicular dysfunction in mouse testis cells by dysregulating calcium homeostasis and stimulating endoplasmic reticulum stress. Sci Total Environ 702:134775. https://doi.org/10.1016/j.scitotenv.2019.134775
35. Li Y, Jin L, Li Y et al (2022) Lysophosphatidic acid improves human sperm motility by enhancing glycolysis and activating L-type calcium channels. Front Endocrinol (Lausanne) 13:896558. https://doi.org/10.3389/fendo.2022.896558
36. Liu X, Teng Z, Wang Z et al (2022) Expressions of HSPA1L and HSPA9 are associated with poor sperm quality of low-motility spermatozoa in fertile men. Andrologia 54:e14321. https://doi.org/10.1111/and.14321
37. Park Y-J, Pang M-G (2021) Mitochondrial functionality in male fertility: from spermatogenesis to fertilization. Antioxidants (Basel) 10:98. https://doi.org/10.3390/antiox10010098
38. Tang W, Xiao Y, Long Y et al (2021) Sodium fluoride causes oxidative damage to silkworm (Bombyx mori) testis by affecting the oxidative phosphorylation pathway. Ecotoxicol Environ Saf 218:112229. https://doi.org/10.1016/j.ecoenv.2021.112229
39. da Silva J, Gonçalves RV, de Melo FCSA et al (2021) Cadmium Exposure and testis susceptibility: a systematic review in murine models. Biol Trace Elem Res 199:2663–2676. https://doi.org/10.1007/s12011-020-02389-0
40. Shih H-J, Chang C-Y, Huang I-T et al (2021) Testicular torsion-detorsion causes dysfunction of mitochondrial oxidative phosphorylation. Andrology 9:1902–1910. https://doi.org/10.1111/andr.13068
41. Dibley MG, Formosa LE, Lyu B et al (2020) The mitochondrial acyl-carrier protein interaction network highlights important roles for LYRM family members in complex I and mitoribosome assembly. Mol Cell Proteomics 19:65–77. https://doi.org/10.1074/mcp.RA119.001784
42. Zhang R, Hou T, Cheng H, Wang X (2019) NDUFAB1 protects against obesity and insulin resistance by enhancing mitochondrial metabolism. FASEB J 33:13310–13322. https://doi.org/10.1096/fj.201901117RR
43. Hou T, Zhang R, Jian C et al (2019) NDUFAB1 confers cardioprotection by enhancing mitochondrial bioenergetics through coordination of respiratory complex and supercomplex assembly. Cell Res 29:754–766. https://doi.org/10.1038/s41422-019-0208-x
44. Chakraborty B, Bhakta S, Sengupta J (2016) Mechanistic insight into the reactivation of BCAII enzyme from denatured and molten globule states by eukaryotic ribosomes and domain V rRNAs. PLoS One 11:e0153928. https://doi.org/10.1371/journal.pone.0153928
45. Branco AT, Lemos B (2014) High intake of dietary sugar enhances bisphenol A (BPA) disruption and reveals ribosome-mediated pathways of toxicity. Genetics 197:147–157. https://doi.org/10.1534/genetics.114.163170
46. Shen X, Yin L, Pan X et al (2020) Porcine epidemic diarrhea virus infection blocks cell cycle and induces apoptosis in pig intestinal epithelial cells. Microb Pathog 147:104378. https://doi.org/10.1016/j.micpath.2020.104378
47. Huang G, Li H, Zhang H (2020) Abnormal expression of mitochondrial ribosomal proteins and their encoding genes with cell apoptosis and diseases. IJMS 21:8879. https://doi.org/10.3390/ijms21228879
48. Guan X, Zhang H, Qin H et al (2020) CRISPR/Cas9-mediated whole genomic wide knockout screening identifies mitochondrial ribosomal proteins involving in oxygen-glucose deprivation/reperfusion resistance. J Cell Mol Med 24:9313–9322. https://doi.org/10.1111/jcmm.15580
49. Zhou Q, Hou Z, Zuo S et al (2019) *LUCAT1* promotes colorectal cancer tumorigenesis by targeting the ribosomal protein L40-MDM 2-p53 pathway through binding with UBA *52*. Cancer Sci 110:1194–1207. https://doi.org/10.1111/cas.13951
50. Carracedo S, Briand-Amirat L, Dordas-Perpinyà M et al (2022) ProAKAP4 protein marker: towards a functional approach to male fertility. Anim Reprod Sci 247:107074. https://doi.org/10.1016/j.anireprosci.2022.107074
51. Fang X, Huang L-L, Xu J et al (2019) Proteomics and single-cell RNA analysis of Akap4-knockout mice model confirm indispensable role of Akap4 in spermatogenesis. Dev Biol 454:118–127. https://doi.org/10.1016/j.ydbio.2019.06.017
52. Zhao W, Li Z, Ping P et al (2018) Outer dense fibers stabilize the axoneme to maintain sperm motility. J Cell Mol Med 22:1755–1768. https://doi.org/10.1111/jcmm.13457
53. Hoyer-Fender S (2022) Development of the connecting piece in ODF1-deficient mouse spermatids. IJMS 23:10280. https://doi.org/10.3390/ijms231810280
54. Sarkar S, Yadav S, Mehta P et al (2022) Histone methylation regulates gene expression in the round spermatids to set the RNA payloads of sperm. Reprod Sci 29:857–882. https://doi.org/10.1007/s43032-021-00837-3
55. Paclik D, Danese S, Berndt U et al (2008) Galectin-4 controls intestinal inflammation by selective regulation of peripheral and mucosal T cell apoptosis and cell cycle. PLoS One 3:e2629. https://doi.org/10.1371/journal.pone.0002629
56. Cao Z-Q, Guo X-L (2016) The role of galectin-4 in physiology and diseases. Protein Cell 7:314–324. https://doi.org/10.1007/s13238-016-0262-9